Black carbon and organic carbon in aerosol particles from crown fires in the Canadian boreal forest

Joseph M. Conny

Atmospheric Chemistry Group, Surface and Microanalysis Science Division, National Institute of Standards and Technology, Gaithersburg, Maryland, USA

John F. Slater

Climate Change Research Center, Institute for the Study of Earth, Oceans, and Space, University of New Hampshire, Durham, New Hampshire, USA

Received 19 September 2000; revised 24 October 2001; accepted 12 November 2001; published 6 June 2002.

[1] In the boreal forest, high-intensity crown fires account for an overwhelming proportion of the area burned yearly. Quantifying the amount of black carbon (BC) from boreal crown fires in Canada is essential for assessing the effect on regional climate from natural wildfire aerosol emissions versus that from anthropogenic activities. This is particularly relevant because climate change will likely lead to increased wildfire activity in northern Canada. During 4–5 July 1998, two controlled fires in Northwest Territories, Canada, were conducted as part of the International Crown Fire Modeling Experiment. We report here the BC and organic carbon (OC) compositions of aerosols produced during the flaming and smoldering stages of burning. Particles were collected on back-to-back quartz-fiber filters by helicopter with a hi-vol sampler and at ground level with a dichotomous sampler to separate the fine ($\leq$2.5 μm diameter) and coarse (2.5–10 μm diameter) particle fractions. An analysis of the back filter in relation to the front filter from the dichot sampler for both the fine and coarse fractions provided a means to correct for the adsorption of gas-phase organic compounds on filters (positive artifact) and for the loss of particulate carbon from filters by volatilization (negative artifact). BC and OC masses, which combine here to give total carbon (TC), were determined by the thermal-optical method. The BC to TC ratio for the flaming stage was 0.085 ± 0.032 ($\bar{x} \pm ksn^{-1/2}$, $k = 2$, $n = 2$), based on aerial sampling of the dark plume 300–500 m above the flame front. BC/TC for the smoldering stage was 0.0087 ± 0.0046 from ground-based sampling. Uncertainties consist of the combined variances in measurement and sampling and in emissions from different fires. These averages and uncertainties serve as important aerosol data input for predictions of climate change on both global and regional scales. *INDEX TERMS:* 0305 Atmospheric Composition and Structure: Aerosols and particles (0345, 4801); 0345 Atmospheric Composition and Structure: Pollution—urban and regional (0305); 0360 Atmospheric Composition and Structure: Transmission and scattering of radiation; *KEYWORDS:* atmospheric particles, boreal forest fires, biomass burning, climate change, black carbon, elemental carbon

1. Introduction

[2] The last 2 decades have revealed the major impact on Earth's atmosphere from large-scale biomass burning, in particular, burning caused by humans [*Crutzen et al.*, 1979; *Crutzen and Andreae*, 1990; *Levine*, 1990]. CH_3Cl and CH_3Br from fires lead to stratospheric O_3 depletion. NO, CO, CH_4, and nonmethane hydrocarbon emissions lead to an increase in tropospheric O_3. CO_2, CH_4, and N_2O from global biomass burning contribute to climate change. Aerosols from biomass burning also affect climate but in complex ways. Atmospheric warming occurs when the black carbon (BC) component (also known as elemental carbon, graphitic carbon, or light-absorbing carbon) in aerosols absorbs solar radiation and then reradiates in the infrared (shortwave heating) or when surface-released heat is trapped by atmospheric aerosols (longwave heating). Cooling occurs when particles scatter solar radiation or when particles provide condensation nuclei for solar-scattering clouds (indirect radiative forcing). Direct radiative forcing includes effects of both the absorption and scattering of solar radiation.

0148-0227/02/2001JD001528$09.00

[3] Aerosol radiative forcing depends upon a number of aerosol parameters such as optical depth (thickness), aerosol size, single-scattering albedo, fraction of light scattered upward, aerosol layer height, and surface reflectance [*Chylek and Coakley*, 1974; *Haywood and Shine*, 1995; *Hansen et al.*, 1997, 1980]. Single-scattering albedo, i.e., the ratio of the scattering coefficient to the sum of the scattering and absorption coefficients, depends to a large extent on aerosol composition. The absorption coefficient, in particular, is approximately proportional to the BC content of aerosols [*Reid et al.*, 1998]. Estimates of the single-scattering albedo of carbonaceous aerosols range from 0.85 to 0.95 [*Liousse et al.*, 1996; *Penner et al.*, 1992]. Above surfaces with equal reflectances the warming affect of aerosols increases as the single-scattering albedo decreases. *Hansen et al.* [1997] determined that the critical single-scattering albedo at which the temperature forcing effect of aerosols shifts from cooling to warming occurs between ~0.86 and 0.91.

[4] Outside of the arctic zone it has been assumed that aerosols generally cause a negative forcing of the global mean temperature, including the largely carbonaceous aerosols from biomass burning. Recent estimates, however, have shown a decrease in the size of direct radiative forcing (W m^{-2}) from biomass burning aerosols. An initial estimate of the direct radiative forcing reported by *Hobbs*

et al. [1997] was -0.8 W m^{-2}, based on work by *Penner et al.* [1992], while an estimate based on more recent measurements was -0.3 W m^{-2} [*Hobbs et al.*, 1997]. More recently, *Haywood and Ramaswamy* [1998] estimated the direct forcing from BC alone at 0.4 W m^{-2}. Thus aerosols may not mitigate the effect of global warming due to greenhouse gases as much as originally thought. For the past decade, aerosols have been known to be the main source of uncertainty in models that predict global warming [*Hansen and Lacis*, 1990]. This uncertainty in the forcing estimates has remained high, by a factor of 2–3 times the estimated value [*Penner et al.*, 1992; *Hobbs et al.*, 1997; *Haywood and Ramaswamy*, 1998], much higher than uncertainty in the radiative forcing by CO_2.

[5] Most studies on global effects of biomass burning have focused on human-caused burning in the tropics. However, large-scale lightning-ignited wildfires are common in the boreal zone (45°N–75°N) of Canada and Siberia. In contrast to radiative forcing by CO_2 the effect of aerosols on climate varies greatly by region [*Kiel and Briegleb*, 1993; *Taylor and Penner*, 1994]. Even though very little (1–2%) of the total carbon (TC) in the global atmosphere is released from burning in boreal regions, models of the BC distribution suggest that burning in the boreal forest may contribute 20–50% of the BC observed in the Arctic in July [*Cooke and Wilson*, 1996]. Thus BC emissions from boreal burning likely affect radiative forcing in the Arctic and sub-Arctic quite differently than burning in other regions. Global climate models may also not represent burning in the boreal forest adequately. In a model of the distribution of aerosols from biomass burning by *Liousse et al.* [1996], calculated aerosol concentrations at key sites in Greenland and Barrow, Alaska, failed to match observations possibly because boreal wildfires were not included in the model.

[6] Of mounting concern is the increase in burn activity in the boreal zone. During 1930–1960, ~6000 fires were detected in Canada, while almost 10,000 fires were detected during the 1980s [*Stocks*, 1991]. Fire statistics also suggest a yearly increase in the burn area and the number of fires in the Canadian territories for 1970–1995 (National Forest Database Program, Canadian Council of Forest Ministers, Natural Resources Canada, 2000, available at http://nfdp.ccfm.org). These increases certainly reflect expanded fire protection capability, growing population, and increased forest use. Nevertheless, increased boreal fire incidence is likely linked to climate change. Climate models suggest that if global CO_2 doubles, the area of Canadian forest subjected to wildfires each year could increase by ~40% [*Flannigan and Van Wagner*, 1991], and the average fire season in Canada could increase by 22% [*Wotton and Flannigan*, 1993].

[7] The quantity and composition of biomass combustion particles depend upon several factors including the composition and size of the fuel, terrain, and weather. In addition, the duration of flaming versus smoldering must be considered [*Lobert and Warnatz*, 1993]. Thus different amounts of BC and organic carbon (OC) in particles from different fire environments are expected (boreal forest versus the tropical savanna). Burning in the tropics produces relatively low BC/TC ratios (0.04–0.06) compared to fossil fuel combustion [*Cachier et al.*, 1989a]. However, the Cachier et al. data suggest that BC/TC ratios for savanna burning are higher than for forest burning, which is consistent with the fact that savanna fires produce copious black smoke during a more predominant flaming stage compared to forest burning. A comparison of BC/TC ratios and the ^{13}C content of biomass burning aerosols by Cachier et al. suggests that combustion properties of tropical savanna burning (i.e., duration of flaming versus smoldering) may be distinctive and distinguishable from the combustion properties of forest burning.

[8] In the boreal forest, high-intensity fires that reach into the forest crown account for an overwhelming proportion of the area burned each year. During 4–5 July 1998, two controlled burns in a primarily jack pine forest near Fort Providence, Northwest Territories, Canada, were conducted by the Canadian Forest Service and the Northwest Territories Department of Natural Resources. The burns were part of the International Crown Fire Modeling Experiment, an ongoing summertime experiment designed to study the properties of high-intensity crown fires. We report here the BC and OC content of combustion particles from the experiment, along with BC/TC ratios, and we include critical uncertainties from measurement error, sampling error, and variation in fire emissions. Corrections were also made for artifacts that arose from the adsorption of gas-phase organic compounds on the sample substrate and from the volatilization or reentrainment of the collected particles.

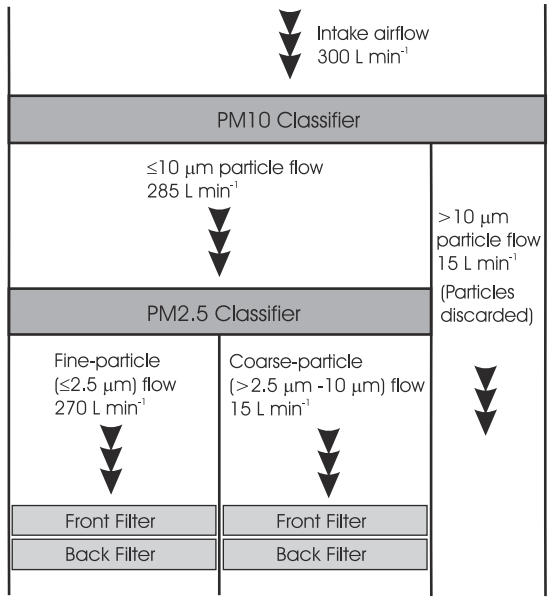

Figure 1. Schematic diagram of the virtual impactor (dichot) used for particle sampling at ground level. The PM10 classifier discards particles >10 μm. Particles smaller than 10 μm are further separated into the fine and coarse fractions by the PM2.5 classifier. For each fraction the front quartz-fiber filter is stacked directly on top of the back quartz-fiber filter. The textured side of the filter is upstream.

2. Methods

[9] During the burn experiment, combustion particles were collected at ground level and by aircraft. For the two burn events we used an MSP Model 310 Virtual Impactor (dichot) for ground-level sampling of fine (≤2.5 μm aerodynamic diameter) and coarse (>2.5–10 μm aerodynamic diameter) particles. (Certain commercial products are identified here to specify the means by which experiments were conducted. Such identification is not intended to imply recommendation or endorsement by the National Institute of Standards and Technology, nor is it intended to imply that the identified product is necessarily the best available for the purpose.) As we discuss in section 3.1, substantial carbonaceous material was collected on the coarse-particle filters during both burn events. Thus the coarse fraction was necessarily included in our mass determinations.

[10] Figure 1 is a simplified diagram of the dicot. Air flowing at 300 L min^{-1} enters the PM10 classifier where particles >10 μm are discarded. Then, the PM2.5 classifier separates the fine and coarse particles. The fine-particle stream is 270 L min^{-1}, while the coarse-particle stream is 15 L min^{-1}. In our study, fine

Table 1. Types of Samples and Sampling Conditions for Aerosols Collected During the 1998 International Crown Fire Modeling Experiment[a]

Date	Sample Type	Equipment	Sampler Height	Duration of Sampling	Additional Details
1 July	background air	dichot	5 m above ground	22.5 hours	no fires observed in the vicinity
2 July	field blank	dichot	5 m above ground	1 min	
4 July	burn, flaming stage	dichot	ground level	15 min	
	field blank	dichot	ground level	1 min	blank for loading of the sampler at the site between the flaming stage and the smoldering stage
	burn, smoldering stage	dichot	ground level	99 min	
	field blank, aircraft	hi-vol	ground level	1 min	blank for loading of the sampler, power not supplied to the sampler
	burn, aircraft	hi-vol	500 m above ground	75–100 s	7–9 passes made through dark plume directly above site
	burn, aircraft	hi-vol	500 m above ground	45–55 s	4–5 passes made through light plume directly above site
5 July	burn, flaming stage	dichot	ground level	21 min	
	field blank	dichot	ground level	1 min	blank for loading of the sampler at the site between the flaming stage and the smoldering stage
	burn, smoldering stage	dichot	ground level	85 min	
	field blank	hi-vol	ground level	1 min	sampler operated in the helicopter at ground level prior to ignition
	burn, aircraft	hi-vol	300–320 m above ground	34 s	three passes made through dark plume directly above burn site
	burn, aircraft	hi-vol	1600 m above ground	35 s	plume followed downwind for ~1.5 km
	burn, aircraft	hi-vol	1600 m above ground	19 s	plume followed downwind for ~1.5 km

[a] Dichot is the MSP Model 310 Virtual Impactor. Fine particles ($\leq$2.5 μm) were collected on 200 mm × 250 mm quartz-fiber filters placed back to back in the sampler. Coarse particles (2.5–10 μm) were collected on 62 mm × 165 mm back-to-back quartz-fiber filters. Hi-vol is the Staplex Model TFIA-4 Air Sampler. Particles were not size-segregated. Particles were collected on 102 mm diameter back-to-back quartz-fiber filters.

particles were collected on 200 mm × 250 mm quartz-fiber filters (Pall-Gellman, TISSUQUARTZ 2500QAT-UP), which were heat treated by the manufacturer for 1 hour at 700°C. Each filter for the fine particles was backed by an identical filter in the dichot (Figure 1). Coarse particles were collected on 62 mm × 165 mm heat-treated quartz-fiber filters and backed by an identical filter in the dichot. Backing filters were installed to account for the condensing of semivolatile compounds on the filter substrate [*Cadle et al.*, 1983; *McDow and Huntzicker*, 1990; *Fitz*, 1990] and for particles from the front filter that may have become volatilized or reentrained and then redeposited on the back filter [*König et al.*, 1980; *Eatough et al.*, 1990]. Prior to traveling to the sampling location, filters were preweighed and packaged in envelopes of aluminum foil. The foil was heated at 500°C for 18 hours prior to packaging.

[11] For aircraft sampling a Bell 204 helicopter was outfitted with a Staplex TFIA-4 Air Sampler (hi-vol) rated to draw 400 L min^{-1}. We used 102 mm diameter quartz-fiber filters that were also heat treated by the manufacturer. Fine and coarse particles were collected on the same filter. As with the ground-based dichot sampler, back-to-back filters were installed.

2.1. Ground-Based Sampling

[12] Table 1 shows the types of samples and collection conditions. For ground-based sampling, separate samples were collected during the flaming stage and the smoldering stage that followed. The dichot was placed in the predicted path of the smoke plume in a cleared tract ~50 m from the end of the experimental plots. During the 4 July experiment, burning advanced slowly at first but eventually developed into a full crown fire. Flames reached the end of the plot in ~10 min. During the next 15 min, sooty black smoke moved out of the plot and into the clearing, as shown in Figure 2, blanketing the dichot, which is barely visible on the right side of the fireguard in the photograph. As flaming subsided on 4 July, the sampler filter holder assembly was brought to a clearing away from the densest smoke where we acquired field blanks by briefly inserting clean filters in the filter holder assembly. Next, we reloaded the sampler and ran it for 99 min to collect particles from the smoldering stage (Figure 3). On 5 July, burning ensued rapidly, with flames reaching the end of the plot in ~3 min. The flaming and smoldering stages were sampled for 21 min and 85 min, respectively.

2.2. Aircraft-Based Sampling

[13] During each burn event, two distinct plumes formed above the burn site: one dark in color and the other light. The dark plume clearly formed directly above the flame front. It contained substantial black smoke and a high proportion of particles from the flame front as it moved through the plot. Thus the dark plume represented the flaming stage of combustion. The light-colored plume clearly formed behind the flame front. It contained a high proportion of particles from smoldering that followed the flame front. Thus the light plume represented the smoldering stage. As indicated in Table 1, each type of plume was sampled by making multiple passes through each plume above the burn site. In addition to above-site sampling, two additional samples were taken on 5 July by passing through the darker plume as the helicopter "chased" the plume from above the burn site to ~1.5 km downwind of the burn site.

2.3. Analysis of BC and OC

[14] To determine the OC and BC masses on filters that would best represent carbon emitted during the course of a crown fire, portions of filter were taken from the center and from the edge of the filter. In this study, most filter samples were analyzed in duplicate (i.e., one section from the center and one from the edge). Exceptions were the background air sample and the two "plume chase" samples where four replicate analyses were made: two sections from the center and two from the opposite edges of the filter.

[15] OC and BC fractions in the particles were analyzed at the National Institute of Standards and Technology by the thermal-optical method [*Birch and Cary*, 1996] employing a Sunset Laboratories' Thermal/Optical Carbon Analyzer. Figure 4 shows a typical thermogram with temperature set points for each step. In this case the sample is fine-particulate matter from the smoldering stage. Sections of particle-laden filters are placed in the sample

Figure 2. View of the 4 July burn as the flame front reaches the end of the plot and sooty smoke extends through the fireguard. Sampling equipment, located on the right side of the fireguard (arrow), is positioned to collect particles from the black plume near ground level shown in the photograph. See color version of this figure at back of this issue.

oven where they are exposed to an inert or an oxidizing atmosphere and heated in two phases to a maximum temperature of 900°C each time. First, OC and carbonate carbon are volatilized in a He atmosphere as the sample oven temperature rises stepwise to 900°C. Carbonate was not detected in our samples. The OC evolved during this phase is defined operationally as volatile OC. In addition, during this phase, pyrolyzed carbon (char) forms on the filter. Next, the oven temperature is reduced to 600°C, the sample is exposed to a 1% O_2 in He atmosphere, and the temperature is again ramped in stages to 900°C. Carbon evolved at the start of this phase is defined operationally as pyrolyzed OC. The gas streams of first the volatile OC and then the pyrolyzed OC enter an adjacent oven containing MnO_2 at 875°C where the material that has evolved up to this point is stoichiometrically oxidized to CO_2. Farther along in the gas stream, the CO_2 is catalytically reduced to CH_4. CH_4 is then detected by a flame ionization detector (FID).

[16] During the process the laser transmission (proportional to transmittance) through the filter at 670 nm is monitored. The largest reduction in transmittance occurs during the charring of OC. As this pyrolyzed OC is removed from the filter, the transmittance rises to its initial value. At this point all OC, volatile and

Figure 3. View of the plot burning on 4 July during the smoldering stage. See color version of this figure at back of this issue.

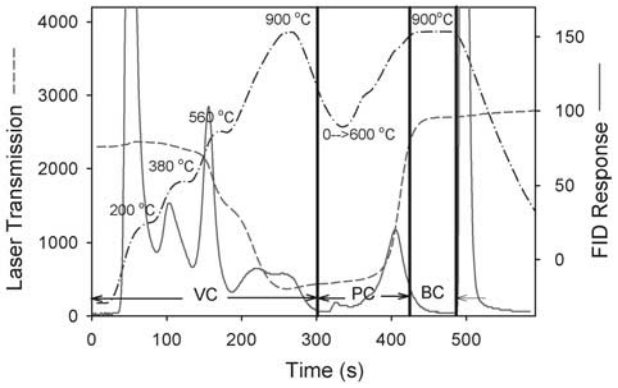

Figure 4. A representative thermogram for organic carbon (OC) and black (BC) from the thermal-optical method. The red dashed line is laser transmission (proportional to transmittance) at 670 nm; the blue dashed-dotted line is temperature (with set points); the green solid line is flame ionization detector (FID) response. The sample is fine-particulate matter collected with the dichot during smoldering on 4 July. OC is first volatilized by heating in steps to 900°C in a He atmosphere. Carbonate carbon is also volatilized if present; however, none was detected. Volatilized carbon (VC) is oxidized to CO_2 then reduced downstream to methane where it is detected by flame ionization, as are all carbon compounds that follow. Pyrolized OC (PC) that formed on the filter in the He atmosphere is removed from the filter in a 1% O_2 in He atmosphere as the temperature is first lowered and then ramped again in steps to 900°C. BC is quantified when the laser transmission rises above the initial transmission of the filter at the split point (424 s). See color version of this figure at back of this issue.

pyrolyzed, has been removed from the filter. As the sample oven temperature continues rising to 900°C, any additional carbon evolving from the filter that causes the transmittance to rise above the initial value is considered the BC component. Thus char from the pyrolysis of OC in the instrument is not included as BC. BC is stoichiometrically oxidized to CO_2 and farther in the stream reduced to CH_4 in the same manner as for the OC.

[17] In this method the standard deviation for a blank containing no known carbon is 0.2 μg C cm^{-2} (R. A. Cary, Sunset Laboratories, Inc., personal communication, 1998). Since the instrument uses filter sections of $\geq$1.0 cm^2, the minimum detectable carbon (OC or BC) is above 0.2 μg. To maximize the amount of carbon detected by the instrument, we used 1.5 cm^2 filter sections. For all samples taken during burning (except the backup filters as discussed in section 3.1), thermograms exhibited measurable FID area even at low carbon levels. For example, in Figure 4 the FID area for BC is quite evident, yet BC was rather low at 0.39 μg cm^{-2}.

2.4. Correction for Adventitious Carbon

[18] Even though we used heat-purified filters for both ground-based and aircraft-based sampling, adventitious OC was still present on the filters. To correct for this blank carbon, we measured OC on center and edge sections from unused filters. Averages and uncertainties in OC mass are shown in Figure 5. Uncertainty bars terminated with narrow caps are the standard deviations for individual OC measurements. Uncertainty bars terminated with wide caps are standard deviations for repeated samplings of the filter blank (n = 4). P_{null} indicates the probability that there is no difference for the OC measurements between the filter center and the edge based on the t test for paired analyses.

[19] For the 200 mm × 250 mm filters in foil envelopes the relatively high levels of OC were likely due to residual carbon on the aluminum foil that remained after heat treatment. Owing to large uncertainties in this case, there was no significant difference in adventitious OC between the center and edge of the filters (P_{null} = 0.62). The 62 mm × 165 mm filters and the 102 mm diameter filters in foil envelopes do, however, show significant differences between the filter center and edge (P_{null} = 0.011 and 0.001, respectively). For both types of filters, OC was higher at the filter edge. Determinations of adventitious OC on filters from the manufacturer's packages are comparable to values reported previously (0.8–1.2 μg cm^{-2}) for quartz-fiber filters that were heated for several hours at 500°C [*Cadle et al.*, 1983]. Thus heat purifying the filters in our lab in preparation for field sampling, in addition to the manufacturer's heat treatment, would likely not have reduced adventitious OC significantly.

3. Results and Discussion

3.1. Filter Artifacts: Ground-Based Sampling

[20] In a comparison of sampling methods for ambient aerosols, *Hering et al.* [1990] found that different sampling methods often produce greater variation in OC results than different carbon measurement methodologies. To a great extent this is due to two sampling artifacts. The adsorption of gas-phase organic matter on the filter substrate leads to an erroneously high OC measurement and is thus a positive artifact. The loss of particles from the filter substrate during sampling, because of volatilization of particulate carbon or perhaps of reentrainment of particles, leads to an erroneously low OC measurement and is thus a negative artifact. Studies have shown that the negative artifact is commonly larger than the positive artifact in ambient aerosols [*Appel et al.*, 1983; *Eatough et al.*, 1990]. One study reported losses averaging 50% of the particulate carbon collected on a hi-vol filter [*Appel et al.*, 1983]. One approach is to employ a backing filter in a hi-vol sampler and to use the OC mass on the back filter to correct for the adsorption of gas-phase organic matter. However, the drawback to measuring carbon on a backing filter to correct for the positive OC artifact is that the backing filter may contain more particulate OC than gas-phase OC.

[21] To assess and correct for both the positive and negative sampling artifacts in this study, we employed information from the

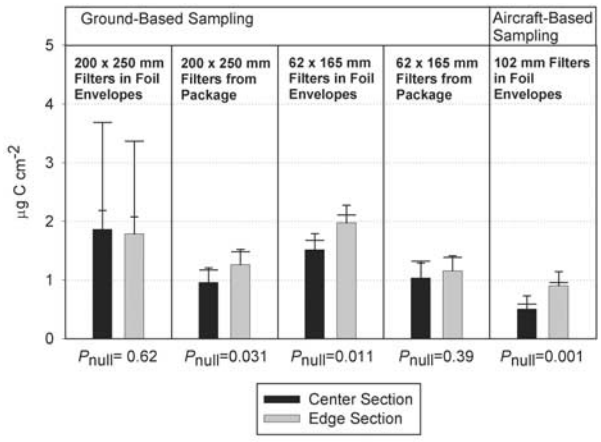

Figure 5. Analysis of OC on center sections and edge sections of filter blanks. The 200 mm × 250 mm filters were used to collect fine particles in the dichot; the 62 mm × 165 mm filters were used to collect coarse particles. All filters were heated at 700°C for 1 hour by the manufacturer. Aluminum foil was heated at 500°C for 18 hours. Uncertainty bars with narrow end caps are standard deviations for individual OC measurements. Uncertainty bars with wide end caps are the standard deviations for repeated samplings of the filter blank (n = 4). P_{null} is the probability at the 5% significance level that no difference in OC exists between the filter center and edge.

Table 2. Ratios of the Pyrolyzed OC Peak Area to the Volatile OC Peak Area and Initial Filter Absorbances at λ = 670 nm From Thermograms

	Flaming Stage				Smoldering Stage			
	July 4		July 5		July 4		July 5	
	Ratio	Absorbance	Ratio	Absorbance	Ratio	Absorbance	Ratio	Absorbance
				Front Filters				
fine particles	0.16	0.202	0.12	0.066	0.12	0.167	0.11	0.178
coarse particles	0.001	0.062	<0.001	0.021	0.034	0.063	0.035	0.064
				Back Filters				
fine particles	0.035	<0.001	0.019	0	0.11	0.018	0.15	0.009
coarse particles	<0.001	<0.001	<0.001	0.001	0.028	<0.001	0.028	0.003

front and back filters of the fine-particle stage as well as information from the front and back filters of the coarse-particle stage (Figure 1). Specifically, we looked at the amounts of volatile OC and pyrolyzed OC from the thermal-optical method (Figure 4) and the initial optical absorbances from the thermograms for each filter. Pyrolyzed OC from this method does not directly indicate particulate mass. However, a filter containing only gas-phase OC would produce only minimal, if any, pyrolyzed OC from the thermal-optical method. The initial filter absorbance from the method does correlate with particulate mass. In Table 2 we show the ratios of the amount of pyrolyzed OC to volatile OC (as area ratios) and the initial filter absorbances at 670 nm from the thermograms. Large OC ratios in Table 2 for the front fine-particle filters (0.16, 0.12, 0.12, and 0.11) indicate substantial particulate OC, as expected. These data are consistent with the corresponding filter absorbances (0.202, 0.066, 0.167, and 0.178), indicating substantial particulate OC. The highest OC ratio (0.16) and the highest absorbance (0.202) are for the front fine-particle filter from the flaming stage on 4 July. The back fine-particle filters for the flaming stage on 4 and 5 July contain small but measurable OC area ratios (0.035 and 0.019); however, these filters did not absorb. Thus, while OC ratios indicate that some particulate carbon may exist on the back fine-particle filters, the amount is negligible. We conclude here that for the flaming stage, loss of particulate carbon (negative artifact) was not significant. However, measurable OC exists on the back fine-particle filter; therefore we must assume that the OC is gas-phase and that it is present on the front filter. Thus a correction for the positive artifact is required in this case.

[22] We can further understand the magnitude of the filter artifacts by assessing the OC mass on the back filters with respect to the OC mass on the front filters. Figure 6 shows the ratios of OC mass on the back filter to OC mass on the front filter. We focus here on the ground-based burn samples. Ratios for the background air sample and the aircraft-based burn samples are shown for comparison. During the flaming stage the amount of OC on the back filter for fine particles was ~10% of that on the front filter (solid bars in Figure 6). In contrast, the amount of OC on the back filter for coarse particles from the flaming phase was much larger, up to 30%, relative to the front filter (shaded bars in Figure 6). As we discuss below, the amount of particulate matter from combustion in the coarse fraction was approximately one third of the particulate matter in the fine fraction. Now, if loss of particulate carbon was the main effect, we would not expect the coarse-fraction filters to have a higher back OC to front OC ratio than the fine fraction. This is because the coarse fraction has much less particulate mass than the fine fraction. We might, on the other hand, expect a higher back OC/front OC ratio for the coarse-fraction filters if the effect is mainly the adsorption of gas-phase OC. This is because there is less particulate mass on the front filter of the coarse fraction to lower the back/front ratio compared to the fine fraction. Thus back/front ratios for the flaming stage in Figure 6 suggest that the gas-phase OC adsorbed significantly on filters during the flaming phase of burning.

[23] In contrast to flaming, the amount of fine-particulate OC on the back filter for the smoldering stage was ~20% of that on the front filter (Figure 6), twice the ratio for the flaming stage. However, OC on the back coarse-particle filter was only ~10% of that on the front filter, nearly one third the ratio for the coarse-particle filter from the flaming stage. Thus the fine versus coarse pattern for the smoldering stage shown in Figure 6 is the reverse of that for the flaming stage. This suggests that there are substantial differences in the relative magnitudes of the positive and negative artifacts between the flaming stage and the smoldering stage.

[24] For the smoldering stage the back fine-particle filters for 4 and 5 July also have high OC ratios (0.11 and 0.15, respectively) in Table 2. However, these filters have measurable (albeit low) absorbances (0.018 and 0.009), indicating that these back fine-particle filters contain small but nonnegligible particulate OC. Thus the fine-particle filters from the smoldering stage must be corrected for loss of particulate carbon as well as adsorbed gas-phase OC. It is important to note that the back coarse-particle filters show essentially no absorbance in Table 2, indicating that particulate OC there is negligible. We used the back coarse-particle OC mass to correct for the artifacts from sampling during the smoldering phase.

[25] The equations used for sampling corrections are shown in Appendix A. Table 3 shows the magnitudes of the positive and negative artifacts as well as the fraction of particulate OC that was collected on the coarse-particle filters from the dichot. The positive artifact was, in fact, a small percentage of the total particulate OC,

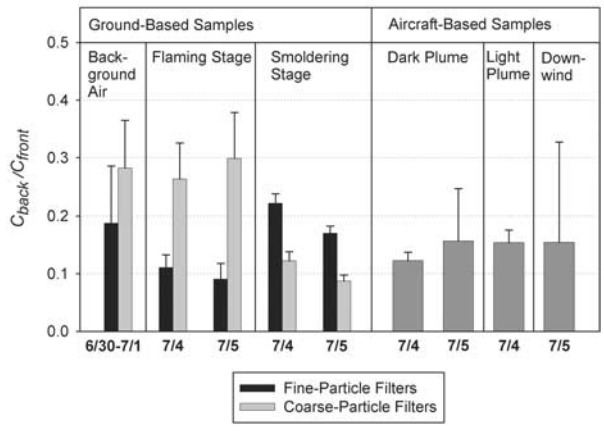

Figure 6. Ratio of the blank-corrected OC mass per unit area on the back filter (C_{back}) to the blank-corrected OC mass per unit area on the front filter (C_{front}). Uncertainty bars show the standard deviation as the combined uncertainty for a ratio involving uncertainty in the respective blank (Figure 5) and uncertainty in an individual OC determination.

Table 3. Size of the Positive and Negative Artifacts and the Amount of OC Collected on the Coarse-Particle Filters as a Percentage of the Total Particulate OC

	Flaming Stage		Smoldering Stage	
	July 4	July 5	July 4	July 5
Positive artifact	4.5	1.1	3.6	2.8
Negative artifact	...	...	8.9	6.4
Coarse fraction	25	26	34	38

ranging from 1.1 to 4.5% for both burn stages. The negative artifact was also rather small, 6.4% and 8.9% for the smoldering stage; however, the magnitude of the negative artifact for the smoldering stage on both burn days was more than twice the size of the positive artifact. The importance of the negative artifact relative to the positive artifact is consistent with studies of particles in ambient air [*Eatough et al.*, 1990].

[26] While our focus in correcting for the loss of particulate carbon was on OC, we observed that the amount of BC on the back filters was statistically insignificant. Thus the loss of particulate OC was proportionately greater than the loss of particulate BC. This suggests that the volatilization of particles, particularly of those particles consisting largely of OC, is a more likely mechanism for the negative artifact than the reentrainment of particles, which would likely affect both OC and BC particles equally.

[27] In contrast to the size of the artifacts the percent of the total carbon in the coarse-particle fraction is relatively large, around 25% for the flaming stage and 34–38% for the smoldering stage. However, this is consistent with results of *Appel et al.* [1983], who reported that 34–44% of the total carbon was in the coarse fraction for ambient air collected with a dichot. In the case of sampling biomass burning aerosols, particles much larger than 2.5 μm that are nonspherical clusters or aggregates of spherical particles <1 μm have been observed in smoke from biomass burning from Brazil [*Martins et al.*, 1998a] and North America [*Cofer et al.*, 1988]. Particle size modes of 1–4 μm, 9–14 μm [*Reid and Hobbs*, 1998], and 20–30 μm [*Andreae et al.*, 1988] from biomass buring in the tropics have been observed. Our results indicate a larger percentage of coarse particles in the smoldering stage.

3.2. Filter Artifacts: Aircraft-Based Sampling

[28] Aircraft-based sampling in our study did not separate the fine particles from coarse particles. Therefore we necessarily based the correction for the positive and negative artifacts on information from the analysis of the fine- and coarse-particle fractions from the dichot (Appendix A). For sampling the dark plume representing the flaming stage, we assumed that only the positive artifact was significant.

3.3. BC/TC Ratios for the Flaming and Smoldering Stages

[29] Uncertainties in our determinations of OC and BC and the BC/TC ratio consist of variance due to sampling uncertainty and measurement uncertainty. We have assumed that uncertainties were independent; thus covariance in the data was not considered. The propagation of these uncertainties was carried out in a robust manner. First, the variance in an individual thermal-optical measurement was combined with the variance in replicate measurements of the appropriate blank (Figure 5). Further, the variance was

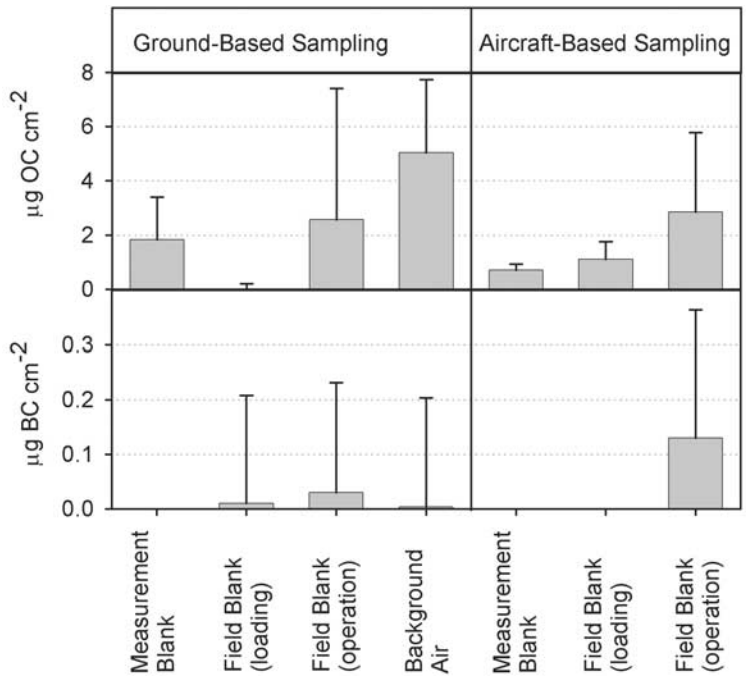

Figure 7. OC and BC compositions of blanks from the 1998 International Crown Fire Modeling Experiment (ICFME). Uncertainty bars show the standard deviation of combined uncertainties as described in the text. The loading blanks provided a control for the change of filters in both the ground-based sampler and the aircraft-based sampler. For the operation field blanks the samplers were operated for 1 min. Background air was sampled for 22.5 hours when no fires were observed.

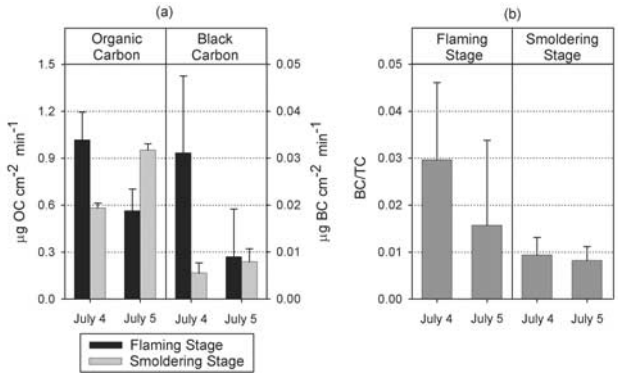

Figure 8. (a) OC and BC filter deposition rates and (b) BC/TC ratios of aerosol particles sampled at ground level during the 1998 ICFME. Uncertainty bars show the standard deviation of combined uncertainties as described in text. The total measured OC for the flaming and smoldering stages on 4 July was 23 ± 4 μg and 87 ± 4 μg, respectively; on 5 July the total measured OC for the two burn stages was 18 ± 4 μg and 121 ± 5 μg, respectively. The total measured BC for the flaming and smoldering stages on 4 July was 0.70 ± 0.37 μg and 0.82 ± 0.32 μg, respectively; on 5 July the total measured BC for the two burn stages was 0.28 ± 0.32 μg and 1.01 ± 0.36 μg, respectively. The fraction of OC from coarse particles was 25–26% of the total particulate OC from the flaming stage and 34–38% of the total particulate OC from the smoldering stage. The fraction of BC from coarse particles was 19–23% from the flaming stage and 18–25% from the smoldering stage. Note the different scales in Figure 8a for OC and BC deposition rates; the OC scale is a factor 30 greater than the BC scale.

sequentially propagated as the replicate measurements (two or four) from the same filter were combined, then artifact-corrected measurements of the front and back filters were combined, finally measurements of the fine and coarse fractions were combined.

[30] OC and BC compositions of field and measurement blanks for both the ground-based and aircraft-based sampling are shown in Figure 7. For comparison, we also show the OC and BC composition in the background air sample. OC levels in the blanks were below the level in the background air sample, and they generally exhibited large relative uncertainties. BC in the blanks was far below the level of reliable quantification.

[31] Figure 8 shows the levels of OC and BC and BC/TC ratios for the ground-level samples. We present the OC and BC levels in Figure 8a based on the quantity of carbon measured from the filter. The vertical bars in Figure 8a show the average rate of carbon deposition on the filters (μg carbon cm^{-2} min^{-1}). This deposition rate is proportional to the average air concentration of the respective carbon component in air. Average air concentrations in this case are irrelevant because smoke plumes are transient and poorly mixed. However, owing to poor mixing and the fact that air flow through the sampler may have varied during sampling, deposition on the filters was not uniform over the sampling period, particularly during the flaming stage. Smoke from the smoldering stage, in contrast, tended to blanket the sampler for longer periods. Sampling in this manner was thus not ideal. However, OC and BC levels reported as average deposition rates allow us to minimize the dependence of these levels on the sampling duration alone. For example, on both burn days the total BC loading on the dichot filters during the smoldering stage was actually higher than the total BC loading during the flaming stage because the dichot ran 4–7 times longer during the smoldering stage than during the flaming stage (Table 1).

[32] There is an additional advantage to reporting average rates of carbon deposition on filters. Figure 8 allows us to compare the relative uncertainties in OC and BC levels for the two burn stages on different burn days to uncertainties in the BC/TC ratios. Use of the filter deposition rate allows us to include only those uncertainties that are relevant to determining uncertainties in BC/TC ratios. For example, the determination of OC mass or BC mass per total particulate mass (TPM) would have an inflated uncertainty from the TPM determination alone and would have no relevance to the BC/TC ratio.

[33] OC levels and BC levels are shown in Figure 8a on different scales. The OC scale is a factor of 30 greater than the BC scale. The intention here is not to compare OC with BC for a particular burn stage but rather to compare the burn stages for a particular carbon component. Because OC levels varied substantially between the two fires, we cannot distinguish a difference in OC emissions between the flaming and smoldering stages.

[34] In contrast to OC levels, BC levels appear higher for the flaming stage than for the smoldering stage, as we would expect. The problem with the BC levels from ground-based sampling during the flaming stage is the large uncertainty. The relative standard deviation in the BC level for the flaming stage on 4 July was 53%, while the BC determination for the flaming stage on 5 July was overshadowed by the uncertainty. These large relative uncertainties are reflected in the BC/TC ratios for the flaming stage in Figure 8b. By comparison, the relative standard deviation in the BC determinations for the smoldering stage during the 4 and 5 July burns are smaller: 40% and 35%, respectively. Moreover, the relative uncertainties in the BC/TC ratios for the smoldering phase, while sizable, are manageable because the relative standard deviations in the OC determinations during the smoldering stage are small (5.1% and 4.3%, respectively). Therefore we conclude that owing to the relative uncertainties our ground-based sampling for a representative BC/TC ratio was successful for the smoldering stage but not for the flaming stage. For the smoldering stage the larger BC/TC ratio (0.0094) was from the 4 July burn. The TPM for this sample was 24 mg, which corresponds to a mass concentration of 0.86 mg m^{-3} and a BC/TPM ratio of 0.0057. However, the percentage of TC to TPM in this sample (60%) is relatively low, as it is in our other samples, owing perhaps to residual water on the

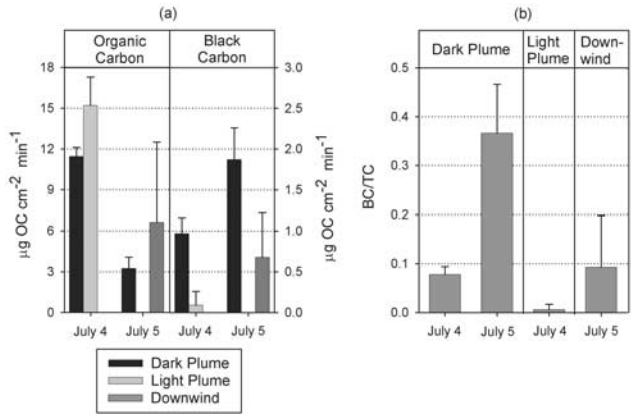

Figure 9. (a) OC and BC filter deposition rates and (b) BC/TC ratios of aerosol particles sampled by aircraft during the 1998 ICFME. Uncertainty bars show the standard deviation of combined uncertainties as described in text. The total measured OC for the dark and light plumes on 4 July was 25 ± 1 μg and 19 ± 3 μg, respectively; on July 5 the total measured OC was 2.8 ± 0.7 μg for the dark plume and 9.9 ± 8.8 μg for the downwind sample. The total measured BC for the dark and light plumes on 4 July was 2.1 ± 0.4 μg and 0.11 ± 0.21 μg, respectively. On 5 July the total measured BC was 1.6 ± 0.3 μg for the dark plume and 0.32 ± 0.26 μg for the downwind sample. Note the different scales in Figure 9a for OC and BC deposition rates; the OC scale is a factor 6 greater than the BC scale.

filter, and thus the 4 July BC/TPM ratio for smoldering may be low.

[35] Levels of OC and BC and the corresponding BC/TC ratios for the elevated plume samples are shown in Figure 9. We find widely varying levels of OC in the darker plume (representing the flaming stage) on 4 and 5 July; however, the OC level in the lighter plume from the 4 July burn was higher than for the darker plume on either day. As expected, BC levels for the darker plume from both burn days are higher than the level for the lighter plume, as well as the downwind sample. Sampling of the dark plume on both days resulted in rather widely varying BC/TC ratios; however, the relative uncertainties are not excessive (21% and 27%, respectively). In contrast to the dark plume samples the BC/TC ratio for the 4 July light plume, representing the smoldering stage, was below reliable quantification, owing to the low and highly uncertain level of BC in this sample. In addition, levels of both BC and OC from the downwind sample on 5 July were too uncertain for a reliable BC/TC estimate. Therefore we conclude that we successfully sampled the flaming stage by aircraft but not the smoldering stage.

[36] Our analysis shows that aircraft-based and ground-based sampling provided complementary means to represent the flaming stage and smoldering stage, respectively, from boreal wildfires. For each burn stage we calculate a variance-weighted mean and a variance-weighed standard deviation for BC/TC. These values are 0.085 ± 0.023 for the flaming stage from aircraft-based sampling and 0.0087 ± 0.0033 for the smoldering stage from ground-based sampling. We also report these ratios with expanded uncertainties U [*Taylor and Kuyatt*, 1994] as follows: 0.085 ± 0.032 for the flaming stage and 0.0087 ± 0.0046 for the smoldering stage, where $U = ksn^{-1/2}$ with k, the coverage factor (analogous to the t statistic), and n both equal to 2.

[37] Since the correction for the negative sampling artifact was based on the analysis of the back filter, it is possible that additional particulate OC was lost from the back filter. Additional OC loss would further lower BC/TC. Therefore the true BC/TC ratios for the fires we sampled, particularly for the smoldering stage, could be lower. However, if we assume that the loss of additional particulate OC is no larger than that found on the back filters in this study (6.4–8.9% of total particulate OC), then the BC/TC ratio may be as low as 0.0081 for the smoldering stage, which is well within the uncertainty for this determination.

3.4. Comparison of BC/TC Ratios With Data From the Literature

[38] A number of studies have derived BC/TC ratios for biomass burning in a variety of plant regions and utilizing a variety of measurement methods. In an overview of biomass burning emissions, *Andreae* [1991] reported that the BC percent by weight of TPM can be as high as 40% for the flaming stage and as low as 4% for the smoldering stage. Clearly, our results are at the low end of this scale or below. Table 4 compares our variance-weighted BC/TC ratios with literature values from a number of field and laboratory experiments. To provide consistency with our analytical approach, we present data from studies that employed the thermal evolution method of carbon measurement, which includes the thermal-optical method, rather than data from studies that employed in situ direct optical methods. Numerous thermal evolution methods have been reported that vary mainly in the maximum temperature and duration of steps in thermally removing

Table 4. BC/TC Ratios From Field and Laboratory Burn Experiments

	Fire Type	Location	Vegetation Type	Sampling Platform	Measurement Method	Flaming Stage	Smoldering Stage
This work	crown fire	Northwest Territories, Canada	boreal forest of black spruce and jack pine	ground-based dichot	thermal-optical		0.0087 ± 0.0046[a]
				helicopter-based hi-vol		0.085 ± 0.032[a]	
Mazurek et al. [1991]	prescribed fire	Ontario, Canada	boreal forest of birch/poplar, fir, and spruce	helicopter-based hi-vol	thermal-optical	0.051	0.045
						0.092	0.011
Martins et al. [1998b]	Cerrado/forest clearing	Brazil	cerrado/tropical forest vegetation (SCAR-B)[c]	fixed-wing aircraft	thermal-chemical[b]	0.054	0.071
							0.044
Andreae et al. [1996]	savanna clearing	South Africa	savanna (SAFARI-92)[d]	ground-based	thermal-chemical	0.084	
Martins et al. [1996]	prescribed fire	Pacific Northwest, United States	cedar debris, Douglas fir/hemlock	fixed-wing aircraft	thermal-chemical	0.082	
						0.13	
						0.10	
						0.12	
						0.077 (wildfire)	
						0.093 (wildfire)	
Patterson and McMahon [1984]	laboratory burn		slash pine needles		thermal-optical	0.29	0.073 (transition)
						0.38	0.026
						0.45	0.017
Currie et al. [1999]	laboratory burn		pine and oak wood		thermal-optical	0.90 to 0.94 (pine)	
						0.86 to 0.88 (oak)	

[a] Variance weighted average and expanded uncertainty U is based on the weighted standard deviation (s). $U = k(s/n^{1/2})$, where $k = 2$ and $n = 2$.
[b] Method of *Cachier et al.* [1989b] was used. See text for details.
[c] SCAR-B is Smoke, Clouds, and Radiation-Brazil (model).
[d] SAFARI-92 is Southern African Fire-Atmospheres Research Initiative.

carbon on filters and in the composition of the carrier gas stream (inert He or N_2, pure O_2, or a combination of He and O_2) [*Novakov and Corrigan*, 1996]. Direct optical methods such as the optical extinction cell and the integrating plate method tend not to agree with thermal evolution methods [*Reid et al.*, 1998]. Differences between our results and the data from field experiments in Table 4 are likely due to a number of factors, in particular, differences in the parameters for the thermal evolution method such as temperature conditions and the type of carrier gases and whether sampling was corrected for artifacts. Corrections for sampling artifacts, if any, were not specified in the studies listed in Table 4.

[39] BC/TC determinations from biomass burning and wildfires in Brazil, South Africa, and the Pacific Northwest in Table 4 utilized the thermal-chemical method of *Cachier et al.* [1989b]. Briefly, filters are first exposed to HCl vapor to remove carbonate. The remaining TC is determined by coulometric titration. BC is analyzed by coulometric titration after removing OC at 340°C for 2 hours under pure O_2. OC is the difference between the determinations for TC and BC. The issue is how the relative distribution of OC and BC in a sample might vary between the thermal-optical and the thermal-chemical method. Large differences in the OC-BC distribution have been observed among the thermal-evolution methods [*Shah and Rau*, 1990], with two factors as the likely main contributors [*Novakov and Corrigan*, 1996]. First is the catalytic effect of Na and K if present at elevated levels in samples. Thermal evolution methods that remove OC under pure O_2 at a constant temperature may be susceptible to premature BC oxidation due to the catalytic effect of the alkali metals. This effect potentially underestimates the BC/TC ratio. The second factor is the underestimation of pyrolysis OC, which then necessarily gets measured as BC. The result is the overestimation of the BC/TC ratio. This second factor affects results when the duration of the thermal program for the pyrolysis stage is inadequate, and less OC is removed under the inert atmosphere than thought. Our thermal-optical method does not appear to overestimate BC by underestimating pyrolysis OC. Generally, our BC/TC results for the flaming stage are consistent with those from a number of field experiments, while our results for the smoldering stage are lower than those reported previously.

[40] Only one set of BC/TC data is known from burning in the Canadian boreal forest. Employing the thermal-optical method for BC and OC on samples collected by aircraft, *Mazurek et al.* [1991] reported 0.051–0.092 for the flaming stage and 0.011–0.045 for the smoldering stage. Our results for the flaming stage derived from aircraft sampling agree with the upper value reported by Mazurek et al. Our results for the smoldering stage derived from ground-based sampling are lower than that of Mazurek et al. but are within the uncertainty range. One reason for the discrepancy is the fact that from our study the negative sampling artifact is larger than the positive artifact. Thus the inclusion of primarily organic particulate material from the back filter from ground-based sampling resulted in a smaller BC/TC ratio compared to results from studies that have not corrected for the negative artifact.

[41] The BC/TC ratios derived from aircraft sampling data of *Martins et al.* [1998b] for the flaming stage of cerrado/forest burning in Brazil are lower, surprisingly, than our results for the flaming stage (0.054) but are substantially higher than our results for the smoldering stage (0.044 and 0.071). However, the data of Martins et al. do not show a consistent difference between the flaming and smoldering stages; a higher BC/TC determination occurs for the smoldering stage than for the flaming stage, indicating mixed-stage sampling. Our results for the flaming stage are similar to those of *Andreae et al.* [1996] for savanna fires in South Africa. However, in this study, a distinction was not made between flaming and smoldering, suggesting, again, that mixed sampling occurred. Our results also fall within the range of data from the flaming stage of prescribed fires in the U.S. Pacific Northwest [*Martins et al.*, 1996].

[42] Laboratory burns of *Patterson and McMahon* [1984] and *Currie et al.* [1999] show much larger BC/TC ratios for the flaming stage than observed in field experiments from our results as well as those of others. Therefore ratios observed in the laboratory are not representative of the flaming stage for forest wildfires or for biomass burning in the tropics. The two BC/TC values of *Patterson and McMahon* [1984] in Table 4 for a distinctive smoldering stage (0.026 and 0.017) are, however, close to values from our field experiments and values of *Mazurek et al.* [1991].

4. Conclusion

[43] We have determined BC and OC compositions of aerosol particles emitted from boreal forest burning during a controlled burn experiment in northern Canada that closely resembled wildfire. The BC/TC ratios determined here for the flaming burn stage (0.085 ± 0.023) and for the smoldering stage (0.0087 ± 0.0033) include robust uncertainties as a weighted standard deviation that involves variances in carbon measurement, sampling, and emissions between different fires. These average ratios and uncertainties serve as important carbonaceous aerosol data input for models that predict long-term climate change on both global and regional scales.

[44] The use of both ground-based and aircraft-based sampling allowed us to select the optimal platform for sampling the flaming stage separately from the smoldering stage. In addition, by collecting size-segregated samples at ground level, and using backup filters in both the ground-based and aircraft-based samplers, we developed a simple method for correcting sampling artifacts that avoided the use of additional field equipment such as a denuder for removing gas-phase OC. As a result of these measurements, our data show a clear distinction in the aerosol BC/TC ratio between the flaming and smoldering stages. The former produced nearly 10 times more BC than the latter, relative to total particulate carbon.

Appendix A

[45] Equations (A1)–(A3) correct for the positive OC artifact for samples from the flaming stage.

$$C_f = C_{f(\text{fine})} + C_{f(\text{coarse})}. \tag{A1}$$

C_f is the total artifact-corrected OC mass per unit filter area for the flaming stage, $C_{f(\text{fine})}$ is the artifact-corrected OC mass for the fine fraction, and $C_{f(\text{coarse})}$ is the artifact-corrected OC mass for the coarse fraction. Each artifact-corrected component is determined as follows:

$$C_{f(\text{fine})} = C_{f(\text{fine front})} - C_{f(\text{fine back})} \tag{A2}$$

$$C_{f(\text{coarse})} = C_{f(\text{coarse front})} - C_{f(\text{coarse back})}, \tag{A3}$$

where $C_{f(\text{fine front})}$ and $C_{f(\text{coarse back})}$ are the blank-corrected OC masses on the front filter. $C_{f(\text{fine back})}$ and $C_{f(\text{fine back})}$ are the blank-corrected OC masses on the back filter.

[46] Equations (A4)–(A6) correct for the positive and negative OC artifacts for samples from the smoldering phase.

$$C_s = C_{s(\text{fine})} + C_{s(\text{coarse})}, \tag{A4}$$

where C_s is the total artifact-corrected OC mass per unit filter area for the smoldering stage. $C_{s(\text{fine})}$ is the artifact-corrected OC mass for the fine fraction, and $C_{s(\text{coarse})}$ is the artifact-corrected OC mass

for the coarse fraction. The artifact-corrected fine-particle component is determined as follows:

$$C_{s(\text{fine})} = \left(C_{s(\text{fine front})} - C_{s(\text{coarse back})}\right)_{\text{pos}} + \left(C_{s(\text{fine back})} - C_{s(\text{coarse back})}\right)_{\text{neg}}. \quad \text{(A5)}$$

The first term on the right-hand side of equation (A5), $(C_{s\,(\text{fine front})} - C_{s\,(\text{coarse back})})$, corrects for the gas-phase positive artifact; the second term, $(C_{s\,(\text{fine back})} - C_{s\,(\text{coarse back})})$, corrects for the particulate-phase negative artifact. $C_{s\,(\text{fine front})}$, $C_{s\,(\text{coarse back})}$, and $C_{s\,(\text{fine back})}$ are the respective blank-corrected OC masses. The coarse-particle component is corrected for the positive artifact only as follows:

$$C_{s(\text{coarse})} = C_{s(\text{coarse front})} - C_{s(\text{coarse back})}. \quad \text{(A6)}$$

Here $C_{s\,(\text{coarse front})}$ is the blank-corrected OC mass for that filter. Combining terms in equations (A4)–(A6) gives the following:

$$C_s = C_{s(\text{fine front})} + C_{s(\text{fine back})} + C_{s(\text{coarse front})} - 3C_{s(\text{coarse back})}. \quad \text{(A7)}$$

In our correction we assume that the front coarse-particle filter for the smoldering stage is saturated with gas-phase OC. This assumption is reasonable because the back coarse-particle filter from the flaming stage contains as much or more OC as the corresponding back fine-particle filter. For example, for the 4 July burn, blank-corrected OC on the back fine-particle filter and on the back coarse-particle filter both measured 0.69 $\mu g\ cm^{-2}$. It appears that during the flaming stage, high levels of gas-phase OC allowed both the fine- and coarse-particle filters to became saturated, even though air flow through the coarse-particle filters was only ~5% of the air flow through the fine-particle filters (Figure 1). During the smoldering stage, levels of gas-phase OC were likely no lower than for the flaming stage because of the pervasiveness of the smoke around the sampler during the smoldering stage. Thus, during the smoldering stage, it is likely that both the fine- and coarse-particle filters were also saturated.

[47] For aircraft-based sampling of the dark plume representing the flaming stage, the correction for the positive OC artifact on the hi-vol filters from sampling of the dark plume is

$$C_{af} = C_{af\,(\text{front})} - C_{af\,(\text{back})}. \quad \text{(A8)}$$

Here C_{af} is the corrected OC mass per unit filter area from the aircraft-based samples for the flaming burn stage, $C_{af\,(\text{front})}$ is the blank-corrected OC mass for the front filter, and $C_{af\,(\text{back})}$ is the blank-corrected OC mass for the back filter. For aircraft-based sampling of the light plume representing the smoldering stage, we assumed the presence of both the positive and negative artifacts as with the ground-based samples. For each burn event we employed the relative magnitudes of the positive and the negative artifacts found from ground-based sampling as follows:

$$C_{as} = C_{as(\text{front})} - 0.28C_{as(\text{back})} + 0.72C_{as(\text{back})}. \quad \text{(A9)}$$

Here C_{as} is the corrected OC mass from the aircraft-based samples for the smoldering stage. $C_{as\,(\text{front})}$ is the blank-corrected OC mass for the front filter, while $C_{as\,(\text{back})}$ is the blank-corrected OC mass for the back filter. Here $0.28C_{as\,(\text{back})}$ is the magnitude of the positive artifact; the factor 0.28 accounts for the proportion of OC mass on the back due to the positive artifact based on equations (A5) and (A6). Here $0.72C_{as\,(\text{back})}$ is the magnitude of the negative artifact; the factor 0.72 accounts for the proportion of OC mass on the back filter due to the negative artifact based on equations (A5) and (A6).

[48] **Acknowledgments.** The authors thank B. J. Stocks and M. E. Alexander of the Canadian Forest Service and R. A. Lanoville of the Government of the Northwest Territories for coordinating the 1998 ICFME. In addition, we thank W. R. Cofer and E. L. Winstead of NASA-Langley for assistance in sampling from aircraft and J. D. Kessler of NIST for assistance in measuring filter properties.

References

Andreae, M. O., Biomass burning: Its history, use, and distribution and its impact on environmental quality and global climate, in *Global Biomass Burning: Atmospheric, Climatic, and Biospheric Implications*, edited by J. S. Levine, pp. 3–21, MIT Press, Cambridge, Mass., 1991.

Andreae, M. O., et al, Biomass-burning emissions and associated haze layers over Amazonia, *J. Geophys. Res.*, *93*, 1509–1527, 1988.

Andreae, M. O., E. Atlas, H. Cachier, W. R. Cofer, G. W. Harris, G. Helas, R. Koppmann, J.-P. Lacaux, and D. Ward, Trace gas and aerosol emissions from savanna fires, in *Biomass Burning and Global Change: Remote Sensing, Modeling and Inventory Development, and Biomass Burning in Africa*, vol. 1, pp. 278–295, MIT Press, Cambridge, Mass., 1996.

Appel, B. R., Y. Tokiwa, and E. L. Kothny, Sampling of carbonaceous particles in the atmosphere, *Atmos. Environ.*, *17*, 1787–1796, 1983.

Birch, M. E., and R. A. Cary, Elemental carbon-based method for monitoring occupational exposures to particulate diesel exhaust, *Aerosol Sci. Technol.*, *25*, 221–241, 1996.

Cachier, H., M.-P. Brémond, and P. Buat-Ménard, Carbonaceous aerosols from different tropical biomass burning sources, *Nature*, *340*, 371–373, 1989a.

Cachier, H., M.-P. Brémond, and P. Bruat-Ménard, Determination of atmospheric soot carbon with a simple thermal method, *Tellus, Ser. B*, *41*, 379–390, 1989b.

Cadle, S. H., P. J. Groblicki, and P. A. Mulawa, Problems in the sampling and analysis of carbon particulate, *Atmos. Environ.*, *17*, 593–600, 1983.

Chylek, P., and J. A. Coakley Jr., Aerosols and climate, *Science*, *183*, 75–77, 1974.

Cofer, W. R., J. S. Levine, D. I. Sebacher, E. L. Winstead, P. J. Rigging, J. A. Brass, and V. G. Ambrosia, Particulate emissions from a mid-latitude prescribed chaparral fire, *J. Geophys. Res.*, *93*, 5207–5212, 1988.

Cooke, W. F., and J. J. N. Wilson, A global black carbon aerosol model, *J. Geophys. Res.*, *101*, 19,395–19,409, 1996.

Crutzen, P. J., and M. O. Andreae, Biomass burning in the tropics: Impact on atmospheric chemistry and biogeochemical cycles, *Science*, *250*, 1669–1678, 1990.

Crutzen, P. J., L. E. Heidt, J. P. Krasnec, W. H. Pollock, and W. Seiler, Biomass burning as a source of atmospheric gases, *Nature*, *282*, 253–256, 1979.

Currie, L. A., G. A. Klouda, B. A. Benner Jr., and K. Garrity, Isotopic and molecular fractionation in combustion; three routes to molecular marker validation, including direct molecular 'dating' (GC/AMS), *Atmos., Environ.*, *33*, 2789–2806, 1999.

Eatough, D. J., N. Aghdaie, M. Cottam, T. Gammon, L. D. Hansen, E. A. Lewis, and R. J. Farber, Loss of semi-volatile organic compounds from particles during sampling on filters, in *Visibility and Particles*, edited by C. V. Mathai, pp. 146–153, Air Waste Manage. Assoc., Pittsburgh, Pa., 1990.

Fitz, D. R., Reduction of the positive organic artifact on quartz filters, *Aerosol Sci., Technol.*, *12*, 142–148, 1990.

Flannigan, M. D., and C. E. Van Wagner, Climate change and wildfire in Canada, *Can. J. For. Res.*, *21*, 66–72, 1991.

Hansen, J. E., and A. A. Lacis, Sun and dust versus greenhouse gases: An assessment of their relative roles in global climate change, *Nature*, *346*, 713–719, 1990.

Hansen, J. E., A. A. Lacis, P. Lee, and W.-C. Wang, Climate effects of atmospheric aerosols, *Ann. N. Y. Acad. Sci.*, *338*, 575–587, 1980.

Hansen, J., M. Sato, and R. Ruedy, Radiative forcing and climate response, *J. Geophys. Res.*, *102*, 6831–6864, 1997.

Haywood, J. M., and V. Ramaswamy, Global sensitivity studies of the direct radiative forcing due to anthropogenic sulfate and black carbon aerosols, *J. Geophys. Res.*, *103*, 6043–6058, 1998.

Haywood, J. M., and K. P. Shine, The effect of anthropogenic sulfate and soot aerosol on the clear sky planetary radiation budget, *Geophys. Res. Lett.*, *22*, 603–606, 1995.

Hering, S. V., et al., Comparison of sampling methods for carbonaceous aerosols in ambient air, *Aerosol Sci. Technol.*, *12*, 200–213, 1990.

Hobbs, P. V., J. S. Reid, R. A. Kotchenruther, R. J. Ferek, and R. Weiss, Direct radiative forcing by smoke from biomass burning, *Science*, *275*, 1776–1778, 1997.

Kiel, J. T., and B. P. Briegleb, The relative roles of sulfate aerosols and greenhouse gases in climate forcing, *Science*, *260*, 311–314, 1993.

König, J., W. Funcke, E. Balfanz, and B. Grosch, Testing a high volume air sampler for quantitative collection of polycyclic aromatic hydrocarbons, *Atmos. Environ.*, *14*, 609–613, 1980.

Levine, J. S., Global biomass burning: Atmospheric, climatic and biospheric implications, *Eos Trans. AGU*, *71*(37), 1075–1077, 1990.

Liousse, C., J. E. Penner, C. Chuang, J. J. Walton, and H. Eddleman, A global three-dimensional model study of carbonaceous aerosols, *J. Geophys. Res.*, *101*, 19411–19432, 1996.

Lobert, J. M., and J. Warnatz, Emissions from the combustion process in vegetation, in *Fire in the Environment: The Ecological, Atmospheric, and Climatic Importance of Vegetation Fires*, edited by P. J. Crutzen and J. G. Goldhammer, pp. 15–37, John Wiley, New York, 1993.

Martins, J. V., P. Artaxo, P. V. Hobbs, C. Liousse, H. Cachier, Y. Kaufman, and A. Plana-Fattori, Particle size distributions, elemental compositions, carbon measurements, and optical properties of smoke from biomass burning in the Pacific Northwest of the United States, in *Biomass and Global Change: Biomass Burning in South America, Southeast Asia, and Temperate and Boreal Ecosystems, and the Oil Fires of Kuwait*, vol. 2, edited by J. S. Levine, pp. 716–732, MIT Press, Cambridge, Mass.,1996.

Martins, J. V., P. V. Hobbs, R. E. Weiss, and P. Artaxo, Sphericity and morphology of smoke particles from biomass burning in Brazil, *J. Geophys. Res.*, *103*, 32051–32057, 1998a.

Martins, J. V., P. Artaxo, C. Liousse, J. S. Reid, P. V. Hobbs, and Y. J. Kaufman, Effects of black carbon content, particle size, and mixing on light absorption by aerosols from biomass burning in Brazil, *J. Geophys. Res.*, *103*, 32,041–32,050, 1998b.

Mazurek, M. A., W. R. Cofer III, and J. S. Levine, Carbonaceous aerosols from prescribed burning of a boreal forest ecosystem, in *Global Biomass Burning: Atmospheric, Climatic, and Biospheric Implications*, edited by J. S. Levine, pp. 258–263, MIT Press, Cambridge, Mass., 1991.

McDow, S. R., and J. J. Huntzicker, Vapor adsorption artifact in the sampling of organic aerosol: Face velocity effects, *Atmos. Environ., Part A*, *24*, 2563–2571, 1990.

Novakov, T., and C. E. Corrigan, Influence of sample composition on aerosol organic and black carbon, in *Biomass Burning and Global Change: Remote Sensing, Modeling and Inventory Development, and Biomass Burning in Africa*, vol. 1, pp. 531–539, MIT Press, Cambridge, Mass., 1996.

Patterson, E. M., and C. K. McMahon, Absorption characteristics of forest fire particulate matter, *Atmos. Environ.*, *18*, 2451–2551, 1984.

Penner, J. E., R. E. Dickinson, and C. A. O'Neill, Effects of aerosol from biomass burning on the global radiation budget, *Science*, *256*, 1432–1434, 1992.

Reid, J. S., and P. V. Hobbs, Physical and optical properties of young smoke from individual fires in Brazil, *J. Geophys. Res.*, *103*, 32,013–32,030, 1998.

Reid, J. S., P. V. Hobbs, C. Liousse, J. V. Martins, R. E. Weiss, and T. F. Eck, Comparisons of techniques for measuring shortwave absorption and black carbon content of aerosols from biomass burning in Brazil, *J. Geophys. Res.*, *103*, 32,031–32,040, 1998.

Shah, J. J., and J. A. Rau, Carbonaceous species methods comparison study: Interlaboratory round robin interpretation of results, final report, Calif. Air Resour. Board, Sacramento, Calif., 1990.

Stocks, B. J., The extent and impact of forest fires in northern circumpolar countries, in *Global Biomass Burning: Atmospheric, Climatic, and Biospheric Implications*, edited by J. S. Levine, pp. 197–202, MIT Press, Cambridge, Mass., 1991.

Taylor, B. N., and C. E. Kuyatt, Guidelines for evaluating and expressing the uncertainty of NIST measurement results, *NIST Tech. Note 1297*, Natl. Inst. of Stand. and Technol., Gaithersburg, Md., 1994.

Taylor, K. E., and J. E. Penner, Response of the climate system to atmospheric aerosols and greenhouse gases, *Nature*, *369*, 734–737, 1994.

Wotton, B. M., and M. D. Flannigan, Length of the fire season in a changing climate, *For. Chron.*, *69*, 187–192, 1993.

J. M. Conny, Atmospheric Chemistry Group, Surface and Microanalysis Science Division, National Institute of Standards and Technology, Gaithersburg, MD 20899-8372, USA. (joseph.conny@nist.gov)

J. F. Slater, Climate Change Research Center, Institute for the Study of Earth, Oceans, and Space, University of New Hampshire, Durham, NH 03824, USA. (jslater@cisunix.unh.edu)

Figure 2. View of the 4 July burn as the flame front reaches the end of the plot and sooty smoke extends through the fireguard. Sampling equipment, located on the right side of the fireguard (arrow), is positioned to collect particles from the black plume near ground level shown in the photograph.

Figure 3. View of the plot burning on 4 July during the smoldering stage.

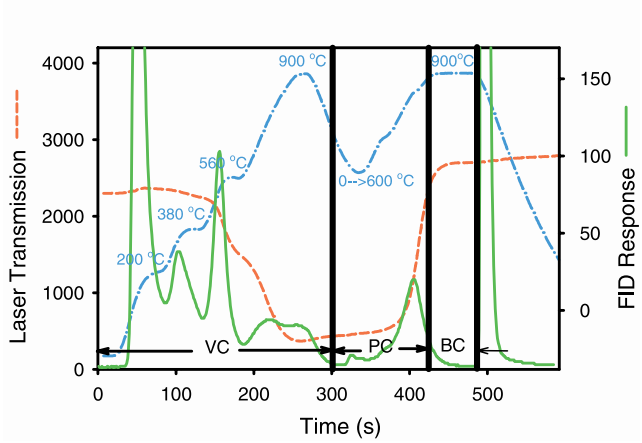

Figure 4. A representative thermogram for organic carbon (OC) and black (BC) from the thermal-optical method. The red dashed line is laser transmission (proportional to transmittance) at 670 nm; the blue dashed-dotted line is temperature (with set points); the green solid line is flame ionization detector (FID) response. The sample is fine-particulate matter collected with the dichot during smoldering on 4 July. OC is first volatilized by heating in steps to 900°C in a He atmosphere. Carbonate carbon is also volatilized if present; however, none was detected. Volatilized carbon (VC) is oxidized to CO_2 then reduced downstream to methane where it is detected by flame ionization, as are all carbon compounds that follow. Pyrolized OC (PC) that formed on the filter in the He atmosphere is removed from the filter in a 1% O_2 in He atmosphere as the temperature is first lowered and then ramped again in steps to 900°C. BC is quantified when the laser transmission rises above the initial transmission of the filter at the split point (424 s).